Nanoparticles

DOI: 10.1002/anie.201000452

Highly Active Iron Oxide Supported Gold Catalysts for CO Oxidation: How Small Must the Gold Nanoparticles Be?**

*Yong Liu, Chun-Jiang Jia, Jun Yamasaki, Osamu Terasaki, and Ferdi Schüth**

Dedicated to Professor Rüdiger Kniep on the occasion of his 65th birthday

Since the pioneering studies of Haruta et al.,[1] CO oxidation over supported gold nanoparticles has become one of the most extensively studied systems in heterogeneous catalysis.[2] Most of the studies have been focused on the origin of the unique catalytic activity of gold nanoparticles. The reasons for this are that on the one hand it is of great scientific interest and on the other hand it may support the development of new catalysts in different fields such as automotive catalysis and polymer electrolyte fuel cells.[3] Specifically, preparation of active gold catalysts[4] influences the size and shape of the gold nanoparticles,[5] the role of the support,[6] the oxidation state of the active gold species (metallic, Au^{+} or Au^{3+}),[7] and the oxygen supply pathways[6a,8]. Unfortunately, however, many reports are highly controversial and the debate is likely to continue for some time owing to the sensitivity and complexity of gold catalysis. Taking the influence of gold particle size as an example, it has been believed that gold nanoparticles of 2–5 nm are the active species for CO oxidation, while Chen and Goodman reported that gold bilayers are more active than the monolayers.[5a] Recently, Hutchings and co-workers used aberration-corrected scanning transmission electron microscopy (STEM) to study iron oxide supported gold catalyst and the activity in CO oxidation was correlated with the presence of gold clusters which are about 0.5 nm in diameter and contain around ten gold atoms.[9]

The origin of this still unclear situation lies—among other factors—mainly in the wide size distribution of gold nanoparticles. By the conventional methods, especially for coprecipitation, typically gold nanoparticles with a wide size distribution of <1 nm to about 20 nm are obtained, which makes the identification of the active species extremely difficult. To help clarify this situation, the colloidal deposition method seems to be more suitable because the gold colloid is already generated before the addition of the support. Furthermore, the size of gold nanoparticles is preserved after the deposition onto the support. Thus, this method has been used to study the effect of the support in gold catalysis.[10] For all the gold catalysts tested, gold nanoparticles were in the size range of around 2–5 nm, as before deposition, and the catalysts showed activities comparable to the gold catalysts synthesized through the deposition–precipitation method.[10] As this method should not result in the formation of smaller clusters, which are described in the literature as the origin of the high activity, the question arose as to whether highly active Au/FeO_x catalysts could be produced by colloidal deposition. This approach would give further clues with respect to the absolute requirement of small clusters for high activity.

To study very small particles in detail, atomic-resolution STEM is probably the most powerful technique because it is capable of characterizing metal clusters of subnanometer dimensions.[9,11] When the high-angle annular dark-field scanning transmission electron microscopy (HAADF-STEM) mode is used, the STEM image can be considered as an incoherent image, and the image intensity increases with the atomic number (Z) of the constituent atoms,[12] therefore even single gold atoms can be observed.[13] Thus, iron oxide supported gold catalysts were synthesized, studied in CO oxidation, and carefully analyzed by HAADF-STEM to obtain precise information on the size and structure of the gold clusters. As will be shown herein, high activity catalysts do not necessarily require the presence of subnanometer gold clusters.

The iron oxide support was synthesized by following a similar procedure as described in the literature.[7b,9] By carefully controlling the synthesis parameters, iron oxide with a Brunauer—Emmett—Teller (BET) surface area of around $260\ m^2 g^{-1}$ can be reproducibly achieved (detailed synthetic procedures are given in the Experimental Section, and N_2 adsorption isotherms of the support are plotted in

[*] Y. Liu, Dr. C.-J. Jia, Prof. Dr. F. Schüth
Max-Planck-Institut für Kohlenforschung
Kaiser-Wilhelm-Platz 1, 45470 Mülheim an der Ruhr (Germany)
Fax: (+49) 208-306-2995
E-mail: schueth@mpi-muelheim.mpg.de
Dr. J. Yamasaki
EcoTopia Science Institute, Nagoya University
Furochou, Chikusa-ku, Nagoya 464-8601 (Japan)
Prof. O. Terasaki
Inorganic & Structural Chemistry and EXSELENT,
Stockholm University
10691 Stockholm (Sweden)
and
Graduate School of EEWS (WCU), KAIST Daejeon
Daejeon 305-701 (Korea)

[**] We thank Dr. E. Okunishi (JEOL) for acquiring STEM images, Prof. G. J. Hutchings and Prof. C. J. Kiely for valuable discussions, B. Spliethoff for the size distribution statistics of the gold nanoparticles, S. Palm for EDX measurements, and Dr. C. Weidenthaler for XRD measurements and helpful discussions. Financial support from the DFG (SFB 558), the Swedish Research Council-VR, the Berzelii Center EXSELENT (Sweden), the World Class University (WCU) program through KOSEF funded by MEST (korea; R31-2008-000-10055-0), and the Alexander von Humboldt Foundation are gratefully acknowledged.

Supporting information for this article is available on the WWW under http://dx.doi.org/10.1002/anie.201000452.

Figure S1 in the Supporting Information). By following the same procedure previously described by our research group,[10] 1 wt% of gold nanoparticles was then deposited onto the iron oxide. The energy-dispersive X-ray (EDX) measurements carried out using scanning electron microscopy (SEM) revealed a gold weight percentage of 1.22%, which is in good agreement with the nominal value. The X-ray diffraction (XRD) patterns of the Au/FeO_x catalyst (Figure S2 in the Supporting Information) indicate that the iron oxide substrate is not well crystalline, which is also confirmed by the STEM images shown later. Also, it is highly possible that the sample contains a mixture of more than one phase (Figure S3 in the Supporting Information). Notably, the reflections of gold cannot be detected because of the low gold loading and small particle size of gold.

The catalytic performance of the Au/FeO_x catalyst thus obtained was then evaluated in CO oxidation, and the CO conversion curves are shown in Figure 1. It can be seen that

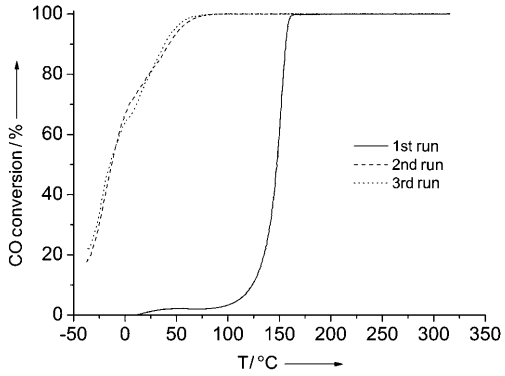

Figure 1. CO oxidation curves of the Au/FeO_x catalyst (1 vol% CO, 20 vol% O_2, rest N_2, space velocity = 80000 mL g^{-1}).

the catalyst first goes through a thermal activation in the first run to burn away the protecting agent, (poly(vinyl alcohol)), which was added during the preparation of the gold colloid. The catalyst shows identical activities in the second and third runs. This outcome is in agreement with previous studies on catalysts produced by colloidal deposition.[10] A $T_{1/2}$ value (temperature at which half conversion of CO is reached) of −14 °C can be observed, thus indicating that the catalyst has a high activity for the low temperature oxidation of CO. Compared with other catalysts that are also synthesized through the colloidal deposition method, the activity of Au/FeO_x is comparable with that of Au/TiO_2, which is probably the best known low-temperature active catalyst for this reaction. For the analogous iron oxide supported gold catalysts prepared by coprecipitation the $T_{1/2}$ value is not given in the literature,[7b,9] instead it was stated that the most active catalyst shows almost full conversion at 25 °C. At this temperature the catalyst reaches 25% conversion at a space velocity of 450000 h^{-1}. We have obtained close to 80% conversion at 25 °C at a space velocity of 80000 h^{-1}. However, when comparing the two systems, one also has to take into account other differences: the gold loading in the current system is significantly lower (1.22 wt% instead of 5 wt%), and the CO concentration in the reaction gas is also different (1 vol% in our case and 0.5 vol% in the literature[9]). Activities of the catalyst synthesized by colloidal deposition and by coprecipitation are thus quite similar—if normalized to the amount of gold in the catalyst.

From the data above, it is obvious that highly active iron oxide supported gold catalyst can be also synthesized through the colloidal deposition method. Here the most interesting question arises: could the activity of the current catalyst also be attributed to gold bilayer clusters with about 0.5 nm in diameter, or are only larger particles with an average size of around 2 nm present?

To answer this question, the Au/FeO_x catalyst was characterized using aberration-corrected STEM in both bright field (BF) and HAADF modes, and representative HAADF-STEM images are shown in Figure 2 (corresponding BF-STEM images and some other images are shown in Figure S4 in the Supporting Information). It can be seen that the iron oxide support is nearly amorphous, which is consistent with the XRD results. It is noteworthy that in certain areas, as shown in Figure 2, many gold nanoparticles

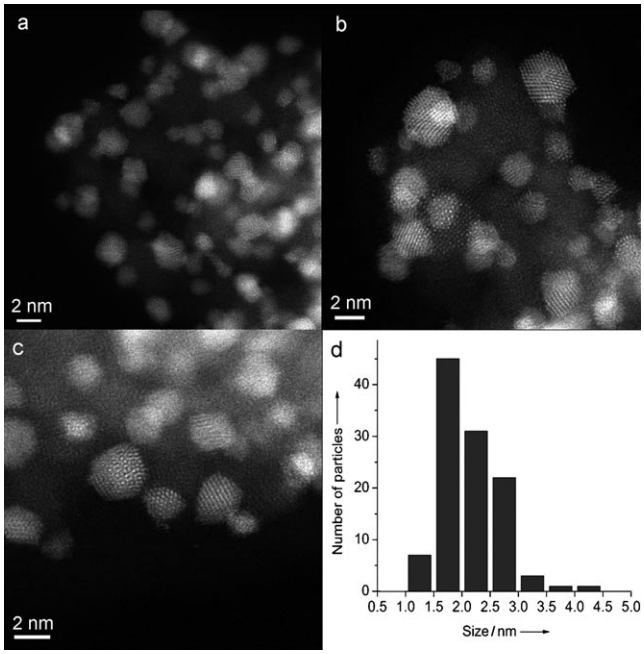

Figure 2. Aberration-corrected HAADF-STEM images and size distribution of the gold particles of Au/FeO_x catalyst prepared by the colloidal deposition method.

can be observed while in some other areas almost no gold particles can be detected. The uneven distribution of the gold nanoparticles has been observed by us in other gold catalysts prepared through the colloidal deposition method,[10a] but the reason for this is not yet clear. However, the most important issue of this study is the size distribution of these particles, and this was thus determined based on Figure 2a–c. In total, 110 particles were found and a mean size of (2.1 ± 0.54) nm was determined. Most significantly, no gold nanoparticles smaller than 1 nm were observed in any of the many images taken. Obviously, it is extremely difficult to disprove the existence of

certain species (especially the extremely small ones like in this case) by microscopy techniques, however, after careful characterization we are confident to claim that no gold clusters of about 0.5 nm are present in the Au/FeO_x catalyst prepared by the colloidal deposition method. Even single atoms can be detected, if they are present. However, gold catalysis is extremely complicated and sensitive, and the current study does not question the observations of previous studies on catalysts prepared by different techniques. This study, however, shows that the small clusters are not crucial for high activity of the catalyst.

The catalysts were also characterized after use in CO oxidation by XRD and STEM (the XRD patterns as well as BF-STEM and HAADF-STEM images are given in Figure S2b and Figure S5 in the Supporting Information, respectively). No changes in the structure of the iron oxide support or the particle size distribution of gold nanoparticles were observed, which is in line with the identical activities in the second and third runs of the catalytic test, and also corresponds to previous studies using this synthetic method.

Another interesting question is: how are the gold atoms packed in the gold particles? It is known that gold bilayer structures are the most catalytically active structure for CO oxidation and some gold nanoparticles around 1 nm have been proposed to have this same structure.[5a,11b] The STEM technique can also give valuable information on this issue: HAADF-STEM images have a lateral resolution on the sub-Å scale and can give a projected image on the Å scale, while at the same time the intensity distribution can provide information on the number of atoms in each atomic column along the beam. If the crystal is thin, it can be expected that the intensity is linearly correlated to the number of gold atoms. In other words, 3D information may be obtained by combining the 2D image and the intensity distributions of the sample. To confirm this assumption, aberration-corrected HAADF-STEM images were simulated under the present experimental conditions (see the Experimental Section) for a Au_{14} cluster model, which consists of four stacked layers in ABCA sequence along [111] and each layer contains 7, 3, 3, and 1 atoms (Figure S6 in the Supporting Information). Figure S7a and S7b show simulated images of this model cluster along [111] and [10$\bar{1}$] projections, and Figure S7c and S7d show intensity profiles along the lines shown by arrows (see the Supporting Information). Similarly, the correlation between the simulated atomic column intensity along [001] and the number of gold atoms can be obtained and is shown in Figure 3. The intensity is roughly proportional to the number of gold atoms up to about six atoms, although slight deviations from linearity are detected. Notably, the increase in intensity is not constant with the increasing number of gold atoms (e.g. the intensity of two overlapping atoms is 2.58 times that of a single atom). However, it is clear that one can still calibrate the number of atoms in every column along the beam, as long as this factor is taken into account. Among typical and well-aligned gold nanoclusters along the incident electron beam, one representative gold cluster with a diameter of 18 Å is shown in Figure 4a. As marked (A, B, E-L) in the figure, several single gold atoms can also be observed. Because the gold catalyst was prepared by the colloidal deposition method, it is highly unlikely that single gold atoms would exist in the colloid, at least not in such a concentration. These single gold atoms are most probably generated by incident electrons during the measurement. Figure S8 in the Supporting Information shows two successively recorded images on the same focus area, and the generation of one single gold atom can clearly be seen —an observation that strongly supports this explanation for the occurrence of single gold atoms. Furthermore, while recording the aberration-corrected HAADF-STEM images we also confirmed that the amount of single gold atoms was increasing with the observation time,

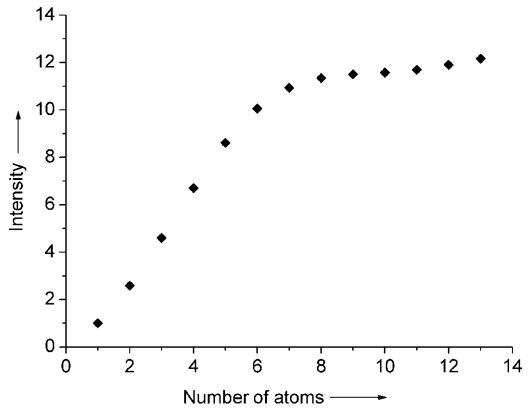

Figure 3. Correlation between simulated atomic column intensity along [001] and the number of gold atoms.

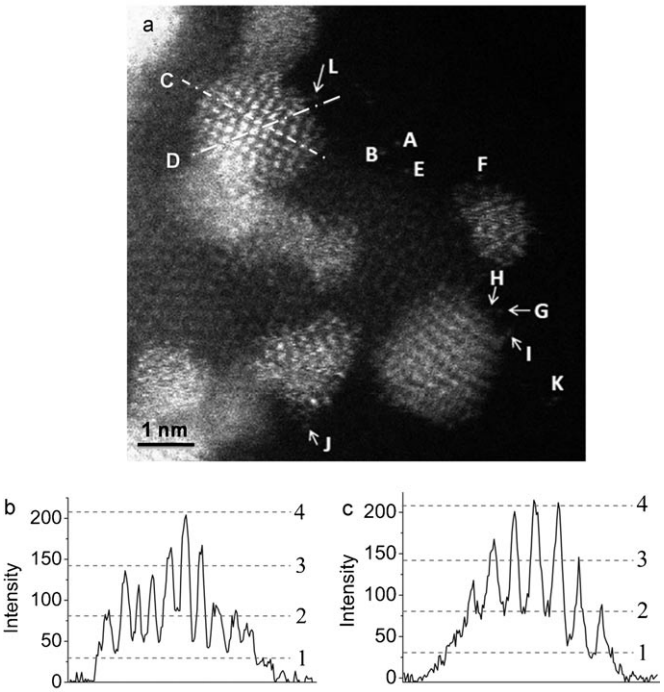

Figure 4. a) HAADF-STEM image of the Au/FeO_x catalyst. Different single atoms (A, B, E-L) are marked. b) and c) The intensity profiles along C and D marked by dashed lines in (a).

and that there was no serious change in the cluster during the time of the observation.

To achieve the standard intensity for a single gold atom, based on which the gold cluster could be studied, the intensity profiles of the ten marked single gold atoms are summarized in Table 1. As can be seen, the intensities vary from 25 to 41,

Table 1: Intensities of different gold single atoms marked in Figure 4a.

Au single atom	Intensity	FWHM [pixel][a]
A	40	5
B	38	6
E	41	5
F	36	8
G	28	8
H	25	7
I	26	6
J	30	8
K	33	6
L	31	6

[a] 1 pixel = 0.16 Å. FWHM = full width at half maximum.

and the average value is 32.8. The reason for the different intensities may result from different focus conditions owing to the different height of gold atoms with respect to the lens, and this variation in intensity can be understood based on the electron probe size through electron optics of the HAADF-STEM technique. The gold atom (L) is the closest to the cluster, and its intensity (31) is also close to the average value. Therefore, the intensity of the gold atom (L) is chosen as the standard for further investigation of the gold cluster. Figure 4b,c shows the intensity profiles of lines C (along [100]) and D (along [110]) after subtracting the background, respectively. Taking 31 as a standard intensity of a single atom and based on the factors between the intensities and increased gold atom numbers given in Figure 3, the theoretical intensities of different gold layers are calculated and indicated by the dashed lines in Figure 4. The quantized nature of the intensities can be seen, and it is clear that the gold cluster has a structure containing up to four gold atoms along the electron beam. Because a variation in the intensities between 25 and 41 was observed for different gold single atoms, both values were then used as standard intensity and the corresponding results are given in Figure S9 in the Supporting Information. Based on these results, we can conclude that the brightest atom columns contain (4±1) atoms along the beam direction, and the possibility that the gold cluster has a bilayer structure can thus be excluded. Haruta and co-workers studied CeO_2 and TiO_2 supported gold catalysts using high-resolution transmission electron microscopy (HRTEM) and HAADF-STEM techniques, and the gold nanoparticles clearly showed multilayer packing, although for these model catalysts no catalytic data is available.[14] Our electron microscopy observation is in agreement with their reports, and, combined with our catalytic data on the same solid, this finally rules out the monolayer or bilayer structure as an absolute requirement for the high catalytic activity in CO oxidation.

Based on the data obtained above, not only the diameter but also the thickness of the gold nanoparticles can be calculated. As the gold particle depicted in Figure 4b,c show, the (4 ± 1) atoms packed in the [100] direction correspond to (12 ± 4) Å, which is close to the diameter of the cluster (18 Å). However, it is very difficult to declare whether the gold nanoparticle is spherical or hemispherical.

In summary, highly active iron oxide supported gold catalysts have been prepared through the colloidal deposition method. HAADF-STEM analyses confirmed that for the current catalyst, gold nanoclusters have diameters larger than 1 nm and that bilayer structures and/or diameters of about 0.5 nm are not mandatory to achieve the high activity. A question one may ask is: what is the active gold species in our system? However, this question can not be answered on the basis of the data that we have collected so far. Nevertheless, the influence of the support, especially the gold–support interaction should probably not be neglected. Actually, in the study of Herzing et al.[9] the major part of the catalytic activity was attributed to very small particles which only comprise about 1–2% of the total gold loading, and based on this assumption a TOF of about $3.5\ s^{-1}$ was calculated. In our catalysts, depending on assumptions about the shape of the gold particles and average size, a TOF of 0.5–1 s^{-1} can be estimated. Thus, although highly active catalysts can be synthesized with gold nanoparticles sized 1 nm and above, there could still be potential for even higher activity—if it were possible to synthesize gold-based catalysts with a high loading that exclusively contained very small gold clusters. In fact, we have reported an extremely active gold-based catalyst having a TOF of approximately $1\ s^{-1}$ at temperatures as low as −89 °C,[8d] but due to the instability of the $Mg(OH)_2$ support in the electron beam of the electron microscopy, sufficiently high resolution to either prove or exclude the presence of bilayer gold particles could not be achieved.

Experimental Section

The iron oxide was prepared through a procedure similar to the one reported by Hutchings and co-workers[9]. Typical procedure for the synthesis of iron oxide: an aqueous solution of $NaCO_3$ (0.25 mol L^{-1}) was added dropwise to 200 mL of aqueous $Fe(NO_3)_3$ (0.1 mol L^{-1}) with stirring at 80 °C until the pH value reached 8.2. The precipitate was then recovered by filtration and washing with 1 L of hot deionized water (80 °C). The material was then dried at 120 °C for 16 h.

The preparation of the Au/FeO_x catalyst by the colloidal deposition method and the catalytic test conditions are the same as described previously.[9] Detailed procedures are outlined in the Supporting Information.

BF-STEM and HAADF-STEM images were acquired on a JEM-ARM200F with a Cs corrector at 200 kV (Cs = 0, convergence angle: 22 mrad, semiangles for HAADF detector: 90–170 mrad, image: 512 × 512 pixels). STEM image simulation was carried out based on the FFT multislice algorithm together with TDS process using xHREM (v 3.0 by HREM Research Inc). Resolutions of HAADF-STEM and BF-STEM images are 0.08 nm and 0.19 nm, respectively. XRD measurements were carried out on a Stoe P diffractometer in transmission geometry with Mo kα1 radiation of 0.70930 Å. Nitrogen adsorption isotherms of the support was measured using an ASAP 2010 adsorption analyzer (Micromeritics) at liquid nitrogen temperature.

Received: January 26, 2010
Revised: May 12, 2010
Published online: July 9, 2010

Keywords: gold · heterogeneous catalysis · iron · nanostructures · oxidation

[1] a) M. Haruta, T. Kobayashi, H. Sano, N. Yamada, *Chem. Lett.* **1987**, 405; b) M. Haruta, N. Yamada, T. Kobayashi, S. Lijima, *J. Catal.* **1989**, *115*, 301.

[2] a) M. Haruta, *Gold Bull.* **2004**, *37*, 27; b) G. J. Hutchings, *Gold Bull.* **2004**, *37*, 3; c) A. S. K. Hashmi, G. J. Hutchings, *Angew. Chem.* **2006**, *118*, 8064; *Angew. Chem. Int. Ed.* **2006**, *45*, 7896; d) B. K. Min, C. M. Friend, *Chem. Rev.* **2007**, *107*, 2709; e) G. C. Bond, D. T. Thompson, *Catal. Rev. Sci. Eng.* **1999**, *41*, 319.

[3] a) X. W. Xie, Y. Li, Z.-Q. Liu, M. Haruta, W. J. Shen, *Nature* **2009**, *458*, 746; b) P. Landon, J. Ferguson, B. E. Solsona, T. Garcia, A. F. Carley, A. A. Herzing, C. J. Kiely, S. E. Golunski, G. J. Hutchings, *Chem. Commun.* **2005**, 3385.

[4] a) S. Tsubota, M. Haruta, T. Kobayashi, A. Ueda, Y. Nakahara, *Stud. Surf. Sci. Catal.* **1991**, *63*, 695; b) W.-C. Li, M. Comotti, F. Schüth, *J. Catal.* **2006**, *237*, 190; c) C. Xu, J. Su, X. Xu, P. Liu, H. Zhao, F. Tian, Y. Ding, *J. Am. Chem. Soc.* **2007**, *129*, 42.

[5] a) M. S. Chen, D. W. Goodman, *Science* **2004**, *306*, 252; b) N. Lopez, T. V. W. Janssens, B. S. Clausen, Y. Xu, M. Mavrikakis, T. Bligaard, J. K. Nørskov, *J. Catal.* **2004**, *223*, 232.

[6] a) M. M. Schubert, S. Hackenberg, A. C. van Veen, M. Muhler, V. Plzak, R. J. Behm, *J. Catal.* **2001**, *197*, 113; b) M. Kotobuki, R. Leppelt, D. A. Hansgen, D. Widmann, R. J. Behm, *J. Catal.* **2009**, *264*, 67; c) B. Yoon, H. Häkkinen, U. Landman, A. S. Wörz, J.-M. Antonietti, S. Abbet, K. Judai, U. Heiz, *Science* **2005**, *307*, 403; d) S. Carrettin, Y. Hao, V. Aguilar-Guerrero, B. C. Gates, S. Trasobares, J. J. Calvino, A. Corma, *Chem. Eur. J.* **2007**, *13*, 7771; e) S. Carrettin, P. Concepción, A. Corma, J. M. Lopez Nieto, V. F. Puntes, *Angew. Chem.* **2004**, *116*, 2592; *Angew. Chem. Int. Ed.* **2004**, *43*, 2538.

[7] a) J. Guzman, B. C. Gates, *J. Am. Chem. Soc.* **2004**, *126*, 2672; b) G. J. Hutchings, M. S. Hall, A. F. Carley, P. Landon, B. E. Solsona, C. J. Kiely, A. Herzing, M. Makkee, J. A. Moulijn, A. Overweg, J. C. Fierro-Gonzalez, J. Guzman, B. C. Gates, *J. Catal.* **2006**, *242*, 71; c) N. Weiher, E. Bus, L. Delannoy, C. Louis, D. E. Ramaker, J. T. Miller, J. A. van Bokhoven, *J. Catal.* **2006**, *240*, 100.

[8] a) J. Guzman, S. Carrettin, A. Corma, *J. Am. Chem. Soc.* **2005**, *127*, 3286; b) L. M. Liu, B. McAllister, H. Q. Ye, P. Hu, *J. Am. Chem. Soc.* **2006**, *128*, 4017; c) X. Y. Deng, B. K. Min, A. Guloy, C. M. Friend, *J. Am. Chem. Soc.* **2005**, *127*, 9267; d) C.-J. Jia, Y. Liu, H. Bongard, F. Schüth, *J. Am. Chem. Soc.* **2010**, *132*, 1520.

[9] A. A. Herzing, C. J. Kiely, A. F. Carley, P. Landon, G. J. Hutchings, *Science* **2008**, *321*, 1331.

[10] a) M. Comotti, W.-C. Li, B. Spliethoff, F. Schüth, *J. Am. Chem. Soc.* **2006**, *128*, 917; b) M. Comotti, C. Weidenthaler, W.-C. Li, F. Schüth, *Top. Catal.* **2007**, *44*, 275; c) M. Comotti, C. D. Pina, R. Matarrese, M. Rossi, *Angew. Chem.* **2004**, *116*, 5936; *Angew. Chem. Int. Ed.* **2004**, *43*, 5812.

[11] a) P. D. Nellist, S. J. Pennycook, *Science* **1996**, *274*, 413; b) S. N. Rashkeev, A. R. Lupini, S. V. Overbury, S. J. Pennycook, S. T. Pantelides, *Phys. Rev. B* **2007**, *76*, 035438; c) J. H. Kwak, J. Hu, D. Mei, C.-W. Yi, D. H. Kim, C. H. F. Peden, L. F. Allard, J. Szanyi, *Science* **2009**, *325*, 1670.

[12] S. J. Pennycook, D. E. Jesson, *Ultramicroscopy* **1991**, *37*, 14.

[13] N. Shibata, A. Goto, K. Matsunaga, T. Mizoguchi, S. D. Findlay, T. Yamamoto, Y. Ikuhara, *Phys. Rev. Lett.* **2009**, *102*, 136105.

[14] a) T. Akita, M. Okumura, K. Tanaka, M. Kohyama, M. Haruta, *J. Mater. Sci.* **2005**, *40*, 3101; b) T. Akita, K. Tanaka, M. Kohyama, M. Haruta, *Surf. Interface Anal.* **2008**, *40*, 1760.

